

Sensitivity Study of Departure Time Accuracy for Airport Collaboration Decision Making Using Fast-Time Simulation

Yota Iwatsuki[1,2], Akinori Harada[3], Shinichiro Higashino[3]

[1]Next-Generation Technology Group, Mobility & Communications Policy Division, Mitsubishi Research Institute, Inc
[2]Graduate School of Engineering, Student of Department of Aeronautics and Astronautics, Kyushu University
[3]Department of Aeronautics and Astronautics, Kyushu University

Abstract

Airport Collaborative Decision Making (A-CDM) relies on accurate operational time predictions to support effective departure and arrival management. This study develops a fast-time simulation framework to evaluate how departure-time prediction accuracy affects arrival-side airborne waiting at Japanese airports. Using flight plan data stored in CARATS Open Data, trajectories are reconstructed, an iterative no-waiting benchmark is generated, and stochastic departure-time errors are introduced under normal and exponentially modified Gaussian distributions. Prediction accuracy is represented by coverage, defined as the probability that the random departure-time error component falls within a specified tolerance window. A distance-based enroute recovery model is applied so that only residual timing errors affect arrival-side merge-point queueing. Sensitivity analyses are conducted for eight major Japanese arrival airports by varying prediction-error bias, coverage, and random seed. The results show clear airport-dependent sensitivity. RJTT has the largest aggregate waiting-time impact, approaching approximately 400 min/day, followed by RJFF at approximately 250 min/day. In contrast, normalized waiting-time results indicate that RJFF and RJOO are particularly sensitive on a per-flight basis. EMG scenarios produce steeper initial increases in waiting time because of right-skewed error tails, but the relative airport ranking is broadly consistent with the Normal case. Departure-airport attribution shows that RJTT is the dominant departure airport in terms of both total and mean allocated waiting time, followed by RJFF. These results indicate that departure-time prediction accuracy requirements should be airport-specific. The proposed framework quantifies the operational benefit of improving prediction coverage and supports evidence-based prioritization of A-CDM-related investments.

Keywords: A-CDM, Fast-time simulation, Prediction accuracy, Air Traffic Management, Sensitivity analysis

1. Introduction

Air traffic demand is expected to continue increasing in the coming decades [1], making efficient use of airport and airspace capacity increasingly important. In particular, at high-density airports and terminal airspace, small disturbances in departure and arrival times can propagate through traffic flow and lead to airborne holding, arrival delay, additional fuel consumption, and increased controller workload. To mitigate such inefficiencies, Airport Collaborative Decision Making (A-CDM) has been introduced as a framework to improve information sharing and coordinated decision-making among airport stakeholders, including aircraft operators, airport operators, air navigation service providers, and ground handlers [2,3].

A-CDM is closely related to the effective operation of departure and arrival management systems, such as Departure Manager (DMAN) and Arrival Manager (AMAN). While these systems support tactical sequencing and flow management, their performance depends strongly on the predictability of aircraft operations. Among various sources of uncertainty, departure-time prediction error is particularly important because it can propagate to downstream arrival-time uncertainty [2,3]. If the actual departure time deviates from the predicted or planned time, the arrival sequence at the destination airport may become less stable, reducing the effectiveness of arrival management and

potentially increasing airborne waiting near the arrival airport.

In Japan, A-CDM has already been introduced at major airports, including Tokyo Haneda Airport and Narita International Airport [4], and further deployment and operational improvement are expected. However, the operational benefit of A-CDM depends not only on the existence of collaborative procedures and information-sharing platforms, but also on the accuracy of key operational predictions like accuracy of departure time and arrival time[5]. In particular, it remains unclear how accurate departure-time predictions must be in order to achieve meaningful reductions in arrival-side airborne waiting and congestion. This question is especially important for prioritizing future investments in A-CDM, trajectory-based operations, and airport-side prediction systems.

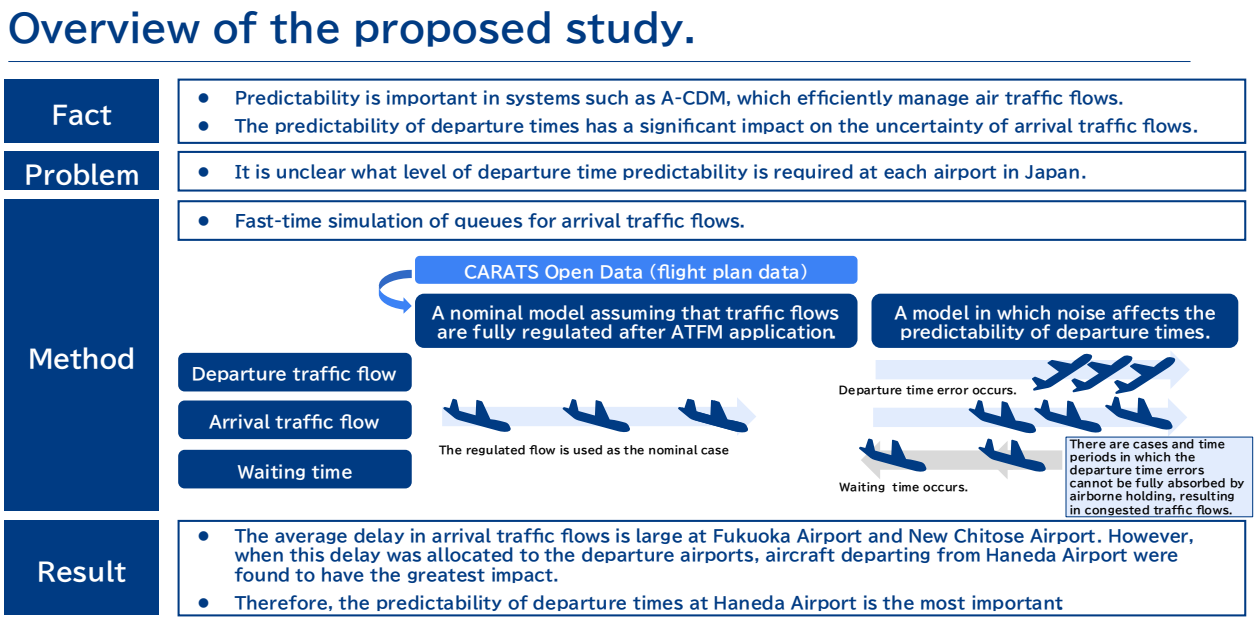


Figure 1. Overview of the proposed study.

Figure 1 Shows the outline of this study. This study addresses this gap by developing a fast-time simulation framework to evaluate how departure-time prediction accuracy affects arrival-side airborne waiting at Japanese airports. Using flight plan data stored in CARATS Open Data, baseline traffic flows are reconstructed and compared with a no-waiting benchmark that represents an idealized, ATFM-smoothed traffic pattern. The benchmark is obtained by iteratively applying the merge-point queueing model to the reconstructed traffic flow and shifting flights with positive waiting time until waiting at the configured merge points is removed or sufficiently reduced. Departure-time prediction errors are then introduced as stochastic parameters, and their residual effects after enroute absorption are propagated to arrival sequencing through a queueing-based simulation. By systematically varying magnitude and distribution of departure-time errors, this study evaluates the sensitivity of airborne waiting time to prediction accuracy on an airport-by-airport basis.

The main contributions of this paper are threefold. First, it proposes a fast-time simulation method for analyzing the relationship between departure-time prediction accuracy and arrival-side airborne waiting using publicly available Japanese air traffic data. Second, it quantifies airport-specific differences in sensitivity to departure-time prediction errors, distinguishing between total delay impacts and mean aircraft delay impacts. Third, it provides a basis for identifying which departure airports may yield greater operational benefits by improved departure-time predictability, thereby supporting evidence-based prioritization of future A-CDM and trajectory-based operation initiatives.

2. Background

2.1 Airport Collaborative Decision Making and Trajectory Predictability

Airport Collaborative Decision Making (A-CDM) is an operational concept designed to improve the efficiency and predictability of airport operations through information sharing and coordinated

decision-making among relevant stakeholders. These stakeholders typically include airport operators, air navigation service providers, aircraft operators, ground handlers, and network management functions. By sharing operational milestones such as target off-block time, start-up approval time, take-off time, and estimated arrival time, A-CDM supports more stable and efficient airport and air traffic flow management.

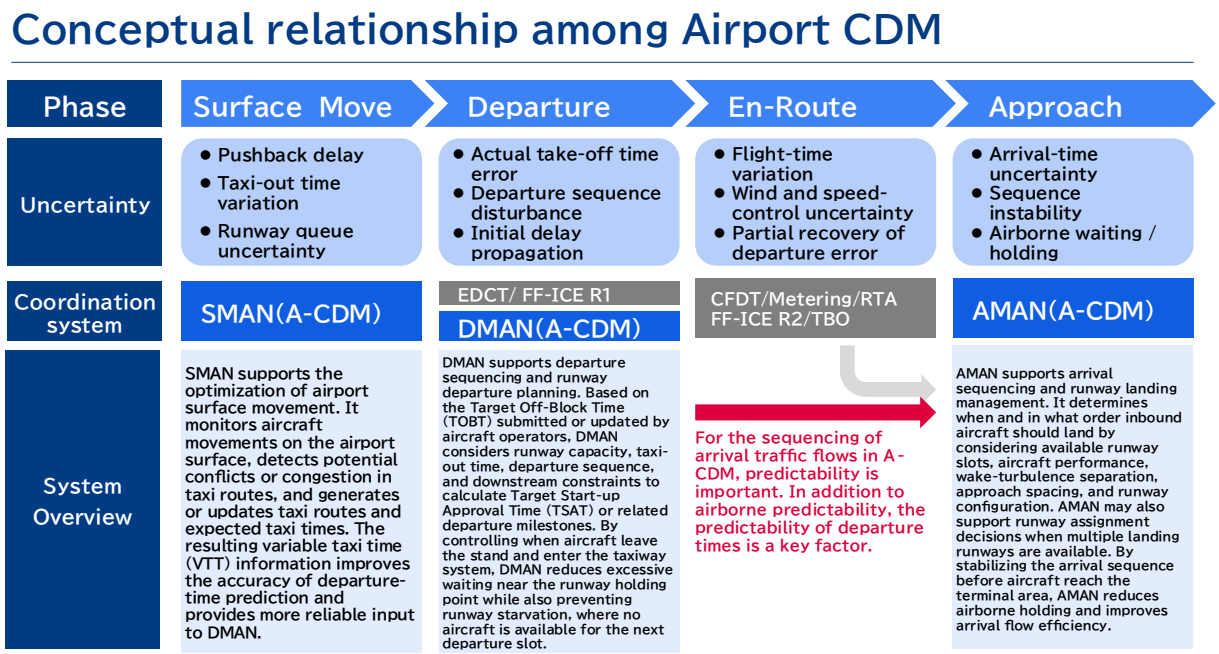


Figure 2. Conceptual relationship among A-CDM

Figure 2 shows relationship between departure management and arrival management in A-CDM. Departure Manager system (DMAN) supports the sequencing and metering of departure traffic by considering constraints such as runway capacity, taxi-out time, and downstream flow restrictions. Arrival Manager system (AMAN), on the other hand, supports the sequencing and spacing of inbound aircraft to reduce arrival delay and airborne holding. Surface Manager system (SMAN) may also support surface movement optimization. These systems are often discussed as complementary components of integrated airport and trajectory-based operations, because departure-side decisions affect not only local airport operations but also downstream airspace and arrival management.

The effectiveness of these systems depends on the predictability of aircraft trajectories. Departure-time uncertainty can affect the accuracy of arrival-time prediction. If an aircraft departs earlier or later than predicted time, part of the error may be absorbed during enroute phase through speed control, route changes, or operational buffers. However, when the residual error remains at the arrival side, it may disturb the arrival sequence and increase the need for airborne waiting or tactical intervention near the destination airport. Therefore, improving predictability of departure-time is not only a departure-side problem, but also an important factor for arrival-side traffic flow management.

2.2 Departure-Time Uncertainty and Existing Studies

Previous studies have addressed several aspects of time uncertainty and traffic flow management relevant to A-CDM. Andreeva-Mori quantified the effects of departure-time prediction uncertainty on Ground Delay Program (GDP) control parameters [6]. Their study modeled departure-time uncertainty and evaluated its impact using cumulative ground delay, airborne delay, and throughput loss as performance indicators. They concluded that modeling departure-time uncertainty is important for selecting appropriate GDP buffer values.

Related domestic research has also examined the trade-off between ground holding and airborne holding under uncertainty [7]. Andreeva-Mori, Matsuno, and Matayoshi considered uncertainties in departure time and enroute flight time when determining departure control timing. Using Monte

Carlo simulations, they evaluated the costs of ground delay, airborne delay, and lost capacity, and showed that an optimal buffer exists for each traffic flow queue.

Enroute time-based metering has also been studied as a mechanism for absorbing part of the required delay during flight [8,9]. Andreeva-Mori and Matsuno evaluated the impact of controlled enroute delays on ground delay distribution for arrival traffic at Tokyo International Airport using real radar and wind prediction data. Their study considered departure-time and flight-time prediction errors and demonstrated the trade-off among ground delay, airborne delay, and capacity loss under different buffer settings. These studies indicate that timing uncertainty, ground delay, and airborne delay should be considered jointly when evaluating traffic flow management performance.

In addition to departure-time uncertainty, flight-time uncertainty has been investigated in the context of four-dimensional trajectory operations[10]. Motodani and Takeichi modeled flight-time variability using actual operational data and showed that uncertainty modeling is indispensable for 4D trajectory operation. This line of research supports the broader importance of modeling time uncertainty in trajectory-based operations.

Although these studies provide important foundations, their main focus is on GDP buffer selection, departure control timing, controlled enroute delay, or flight-time uncertainty modeling. In contrast, the present study focuses on the operational requirement for departure-time prediction accuracy itself. Specifically, it investigates how different levels of departure-time prediction accuracy affect arrival-side airborne waiting and how this sensitivity differs across airports.

This distinction is important for A-CDM implementation. Airport stakeholders need to know not only whether departure-time uncertainty affects traffic flow management, but also what level of prediction accuracy is required to obtain meaningful operational benefits. Moreover, previous studies have mainly examined specific traffic flows or control parameters, whereas the airport-specific sensitivity of Japanese airport operations has not been sufficiently quantified. This study therefore extends prior work by evaluating departure-time prediction accuracy requirements on an airport-by-airport basis using CARATS Open Data and fast-time simulation [11].

2.3 Position of This Study

This study addresses the above gap by evaluating the sensitivity of arrival-side airborne waiting time to departure-time prediction errors on an airport-by-airport basis. Rather than proposing a new prediction algorithm, this paper focuses on the operational requirement side: it investigates how prediction accuracy affects arrival-side performance and how this relationship differs across airports. This distinction is important because prediction models and operational decision-making systems require target accuracy levels in order to assess whether further improvement is operationally meaningful.

To achieve this objective, this study develops a fast-time simulation framework using flight plan data in CARATS Open Data. The framework reconstructs baseline traffic flows, constructs a no-waiting benchmark, introduces stochastic departure-time errors, models enroute absorption, and evaluates the resulting airborne waiting time through a queueing-based arrival simulation. The planned experimental design includes Normal and Ex-Gaussian error models, systematic variation of bias and coverage levels, distance-based enroute absorption, and repeated simulations with multiple random seeds.

Normal distribution is used as a baseline model for symmetric departure-time prediction errors. However, departure operations may also include occasional large positive delays caused by turnaround processes, surface congestion, or tactical flow-management constraints. Such delays can produce a right-skewed error distribution, where most flights remain close to the planned or predicted time, but a smaller number of flights experience relatively large delays. To represent this asymmetric long-tail behavior, this study also uses an Ex-Gaussian distribution. The Ex-Gaussian distribution can be interpreted as the sum of a Gaussian component and an exponential component, and is suitable for representing positively skewed distributions with a long right tail.

This positioning also reflects the intended structure of the full paper. The study first evaluates how departure-time prediction errors affect arrival airports, and then interprets these impacts from the perspective of departure airports, where prediction accuracy improvements would be implemented. The draft presentation emphasizes this transition from arrival-airport sensitivity to departure-airport attribution as a key part of the paper’s story.

3. Methodology

3.1 Overview of the Simulation Framework

This study develops a fast-time simulation framework to evaluate how departure-time prediction errors affect arrival-side airborne waiting. The framework consists of four steps in Figure 3: trajectory reconstruction, construction of a no-waiting benchmark, injection of departure-time errors with enroute absorption, and merge-point queueing simulation.

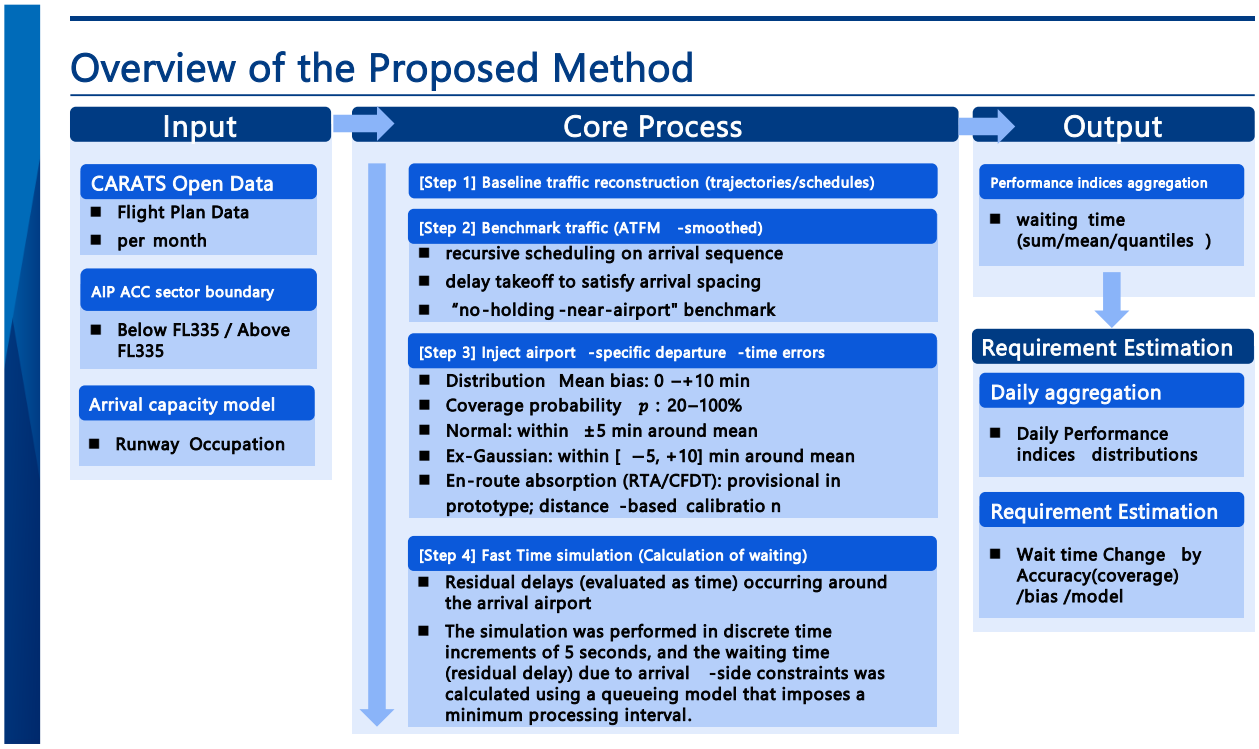


Figure 3. Overview of the fast-time simulation methodology.

First, flight trajectories are reconstructed from CARATS Open data (flight plan data). For each flight, the departure airport, destination airport, departure time, arrival time, estimated elapsed time, and route waypoint sequence are extracted. Waypoint coordinates are parsed from the route information, and waypoint passage times are interpolated according to cumulative route distance. The reconstructed trajectories provide the baseline traffic demand for each arrival airport and analysis day.

Second, a no-waiting benchmark is constructed. This benchmark represents an idealized, ATFM-smoothed reference traffic pattern in which waiting at arrival-side merge points is removed, or at least substantially reduced. Third, stochastic departure-time errors are added to the benchmark traffic flow. A distance-based enroute absorption model is then applied so that only the residual error reaches the arrival-side merge area. Finally, an event-based merge-point queueing simulation is used to calculate airborne waiting time under the assumed spacing constraints.

The purpose of this framework is not to reproduce all tactical air traffic control interventions in detail. Instead, it provides a controlled and interpretable way to quantify the sensitivity of arrival-side waiting to departure-time prediction accuracy.

3.2 Trajectory Reconstruction

Let flight i have a benchmark departure time Di, destination airport ri, and a sequence of waypoints j. The original flight plan data provides departure and arrival times, estimated elapsed time, and route waypoint information. When waypoint coordinates are available, the distance between consecutive waypoints is calculated using geodesic distance. The passage time at each waypoint is then calculated by distributing the elapsed time according to the cumulative distance along the route.

For each analysis day and arrival airport, flights are extracted based on destination airport and

arrival date. The resulting waypoint-level trajectories are used as the input to both the benchmark construction and the sensitivity simulation. Traffic demand is kept fixed across scenarios so that differences in simulation outputs can be attributed to the assumed departure-time error conditions.

3.3 No-Waiting Benchmark

This process continues until total waiting time becomes zero or a predefined maximum number of iterations is reached. The resulting benchmark is used as a reference schedule. Therefore, waiting time generated after adding departure-time errors can be interpreted as waiting induced by prediction uncertainty under the assumed merge-point constraints.

A no-waiting benchmark is constructed before adding departure-time errors. The benchmark is generated through an iterative queue-based adjustment procedure that removes, or substantially reduces, waiting at arrival-side merge points.

For each arrival airport, aircraft are first processed in chronological order of their reconstructed merge-point passage times. At each merge point, a minimum time interval is imposed between consecutive aircraft assigned to the same service lane. If an aircraft reaches the merge point before the selected lane becomes available, the difference is recorded as waiting time.

If waiting occurs, flights with positive waiting times are identified. For each affected flight, the maximum waiting time observed for that flight in the iteration is used as the time shift. The flight's departure time and waypoint passage times are shifted later by this amount. The same queue-based check is then repeated using the shifted trajectory.

This process continues until total waiting time becomes zero or a predefined maximum number of iterations is reached. The resulting benchmark is used as a reference schedule. Therefore, waiting time generated after adding departure-time errors can be interpreted as waiting induced by prediction uncertainty under the assumed merge-point constraints.

3.4 Departure-Time Error and Enroute Absorption

For each scenario, one departure-time error sample is generated for each flight. The simulated departure time D_i^{sim} is given by

$$D_i^{sim} = D_i^{bench} + \epsilon_i \tag{1}$$

where D_i^{bench} is the benchmark departure time and ϵ_i is the sampled departure-time error. The error distribution and its parameters are described in Chapter 4.

Not all departure-time error is assumed to reach the arrival-side merge area. A part of the error may be absorbed during the enroute phase through speed adjustment, route changes, schedule buffers, or tactical control. Therefore, the residual error is defined as

$$\epsilon_i^{res} = \epsilon_i - \alpha_i \tag{2}$$

where α_i is the absorbed portion of the error. In this study, the maximum absorbable amount is modeled as a function of route distance. Longer flights are assumed to have more opportunity to absorb timing errors, while shorter flights are assumed to have less opportunity.

The simulated waypoint passage time $T_{i,j}^{sim}$ is then calculated as

$$T_{i,j}^{sim} = T_{i,j}^{bench} + \epsilon_i^{res} \tag{3}$$

where $T_{i,j}^{bench}$ is the benchmark passage time of flight i at waypoint j. Thus, the full departure-time error affects the simulated departure time, while only the residual error after enroute absorption affects arrival-side sequencing.

3.5 Merge-Point Queueing Simulation

Arrival-side constraints are represented by merge-point queueing. For each arrival airport, a set of merge points is prepared in advance. Each merge point has a waypoint ID, location, number of service lanes, and minimum time interval. The simulation extracts trajectory points whose waypoint IDs match the configured merge points.

Flights are processed in chronological order of simulated merge-point passage time. For each aircraft, the earliest available service lane is selected. If the aircraft reaches the merge point before the lane becomes available, the difference is counted as waiting time. Otherwise, the aircraft passes without waiting.

Let $T_{i,m}^{sim}$ be the simulated passage time of flight i at merge point m, and let $N_{l,m}$ be the next available time of lane l at merge point m. The waiting time is calculated as

$$W_{i,m} = \max\left(0, N_{l,m} - T_{i,m}^{sim}\right) \tag{4}$$

After the aircraft is processed, the lane availability is updated as

$$N_{l,m} \leftarrow T_{i,m}^{sim} + W_{i,m} + S_m \tag{5}$$

where S_m is the minimum interval at merge point m. The waiting time Wim is interpreted as airborne waiting near the arrival-side merge area.

3.6 Performance Indicators

The primary performance indicator is airborne waiting time. For each arrival airport and scenario, total waiting time is calculated as

$$W_r^{total} = \sum_{i,m \in r} W_{i,m} \tag{6}$$

The mean waiting time per merge-point passage event is calculated as

$$W_r^{mean} = \frac{1}{N_r^{event}} \sum_{i,m \in r} W_{i,m} \tag{7}$$

where N_r^{event} is the number of merge-point passage events. In addition, the number of positive waiting events, median waiting time, 90th percentile, 95th percentile, and maximum waiting time are recorded. These indicators are used to evaluate both aggregate impact and delay distribution characteristics.

The simulation outputs are first summarized by arrival airport. Attribution to departure airports is conducted as post-processing using the flight-level waiting-event data, because prediction accuracy improvements are implemented primarily at the departure airport side.

4. Simulation

The numerical experiments were conducted using CARATS Open Data (flight plan data). For each analysis day, flights were grouped by arrival airport based on destination airport and arrival date. The reconstructed waypoint-level trajectories described in Section 3 were used as common traffic demand across all sensitivity scenarios. The target arrival airports were RJGG(Chubu), RJFF(Fukuoka), RJBB(Kansai), ROAH(Naha), RJAA(Narita), RJCC(Shin-Chitose), RJOO(Itami), and RJTT(Haneda).

Departure-time prediction errors were generated by systematically varying distribution type, bias, coverage, and random seed. Two distributions were considered: a normal distribution and an Exponentially Modified Gaussian distribution (EMG). The Normal distribution represents symmetric errors, while the EMG distribution represents asymmetric errors with a right tail. The use of both distributions allows the analysis to distinguish the effect of general dispersion from the effect of rare but large positive departure delays.

In this study, coverage is defined as the probability that the random component of the departure-time prediction error falls within a specified tolerance window. For the Normal distribution, coverage p was defined with respect to the window [−5,+5] min before bias addition. The corresponding standard deviation was calculated as

$$\sigma = \frac{5}{\Phi^{-1}\left(\frac{1+p}{2}\right)} \tag{8}$$

where Φ^{-1} is the inverse cumulative distribution function of the standard Normal distribution. For the EMG distribution, coverage was defined with respect to the window [−5,+10] min before bias addition, reflecting the possibility of larger positive departure delays. The EMG parameters were calibrated numerically so that the specified coverage was satisfied. After adding bias b, the corresponding tolerance windows become [b−5,b+5] min for the Normal distribution and [b−5,b+10] min for the EMG distribution. Coverage was used as the main parameter to describe accuracy because it is easier to interpret operationally than the standard deviation itself. For example, a higher coverage value directly means that a larger proportion of flights depart within the specified tolerance

window.

Bias b was given from 0 to +10 min in 1 min increments, and coverage was given from 20% to 100% in 5 percentage-point increments. Ten random seeds were used for each parameter combination, resulting in 2×11×17×10=3740 scenarios for each airport-day combination. When coverage was set to be 100%, the error was treated as deterministic and equal to the specified bias.

Arrival-side constraints were represented by merge-point spacing. Each arrival airport had a predefined merge-point list, and the default minimum interval was set to be 120 sec. A distance-based enroute absorption model was applied to each departure-time error. Flights with route distances of 200 km or less were assumed to have no absorption capability, while flights with route distances of 1000 km or more could absorb up to 180 sec. For intermediate distances, the absorption limit is assumed to increase linearly with route distance.

The primary performance indicator was airborne waiting time at the configured merge points. For each airport, day, and scenario, the simulation recorded total waiting time, mean waiting time, waiting-event counts, selected percentiles, maximum waiting time, and the number of flights. Sector-count indicators were implemented as optional supplementary outputs but were not used as the primary performance indicators in this paper. Since official airport acceptance rates and sector workload parameters are not publicly available, merge-point spacing was used as a simplified representation of arrival-side sequencing constraints.

Table 1. Experimental settings used in the sensitivity analysis.

Component	Setting
Input data	CARATS-Open Data (flight plan data)
Target arrival airports	RJGG, RJFF, RJBB, ROAH, RJAA, RJCC, RJOO, RJTT
Arrival-side constraint	Merge-point spacing
Default spacing	120 sec
Benchmark	Iterative no-waiting benchmark
Error distributions	Normal, EMG
Bias range	0 to +10 min, 1 min step
Coverage range	20% to 100%, 5 percentage-point step
Coverage window	([-5,+5]) min before bias addition
EMG tail ratio	1
Enroute absorption	Distance-based (Flights with route distances of 200 km or less were assumed to have no recovery capability, while flights with route distances of 1000 km or more could recover up to 180 sec of error. For intermediate distances, the recoverable amount increased linearly with route distance.)
Main indicator	Airborne waiting time
Supplementary indicator	Sector-count proxy, optional

5. Impact of Departure-Time Prediction Accuracy on Arrival-Airport Waiting

5.1 Overview of Arrival-Airport Sensitivity

This section evaluates how departure-time prediction accuracy affects arrival-side airborne waiting at each arrival airport, focusing on total waiting time and mean waiting time per aircraft. The simulation results are first compared across the eight target arrival airports. The objective is to identify airports where prediction errors generate large aggregate waiting time and airports where individual flights are particularly sensitive to such errors.

The figures in this section mainly show the results for the Normal error model with zero bias. The horizontal axis represents the standard deviation σ of the departure-time error distribution. Because σ is calibrated from the coverage parameter defined in Section 4, each point on the horizontal axis corresponds to a specific coverage level. For example, coverage values of 100%, 95%, and 90% indicate that 100%, 95%, and 90% of the random departure-time error component, respectively, fall within the [−5,+5] min tolerance window before bias addition. When coverage is 100%, the error is treated as deterministic and equal to the specified bias; therefore, under the zero-bias condition, σ=0. For visualization, daily values were filtered using the interquartile range (IQR) rule to reduce the influence of extreme outlier days. Specifically, for each airport, distribution type, bias, coverage, and

σ group, daily total waiting-time values outside the interval $[Q_1 - 1.5IQR, Q_3 + 1.5IQR]$ were excluded from the visualization, where Q1 and Q3 are the first and third quartiles and IQR=Q3−Q1. This rule follows the conventional Tukey boxplot outlier criterion [12]. The plotted solid lines show the mean of the retained daily values, dashed lines show the median, shaded bands show the interquartile range, and error bars show the daily standard deviation.

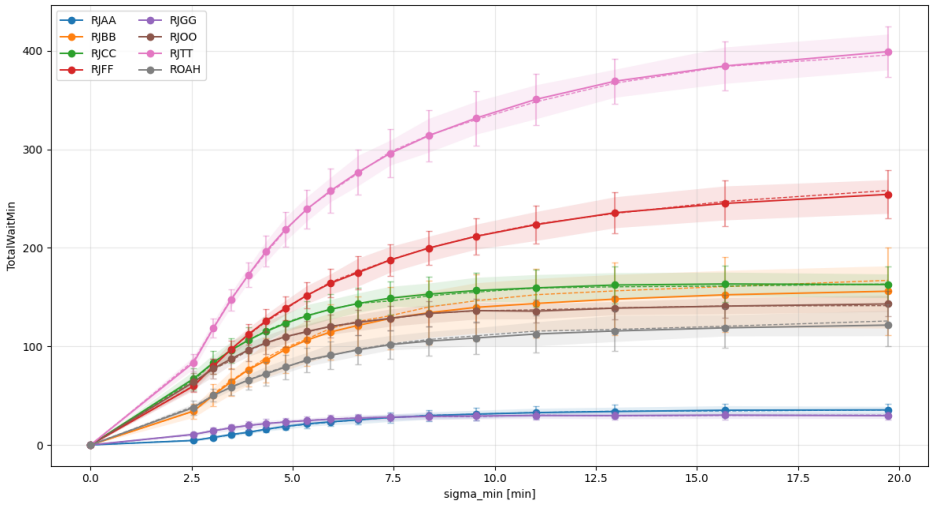


Figure 4. Airport comparison of total daily waiting time under Normal error model with 0 bias.

Figure 4 shows the total airborne waiting time for arrival traffic under the Normal departure-time error model with zero bias. The horizontal axis represents the standard deviation σ of the Normal distribution applied to departure-time errors, and the vertical axis represents the total daily airborne waiting time in minutes. Each point corresponds to a coverage-calibrated value of σ, where coverage indicates the proportion of departure-time errors falling within the [−5,+5] min window before bias is added. In this case, 6.8% of the data were excluded as outliers using the IQR filtering method.

The results show clear airport-dependent differences in total waiting time. RJTT has the largest total airborne waiting time, followed by RJFF and RJCC. This ranking is strongly influenced by traffic volume, because total waiting time represents the aggregate operational burden across all arrival flights. Therefore, high-volume airports tend to have larger total impacts even if the sensitivity of each individual flight is not necessarily the highest.

The curve for RJTT increases rapidly as σ grows from zero and then gradually approaches a plateau. The total waiting time at RJTT asymptotically approaches approximately 400 min per day, while that at RJFF approaches approximately 250 min per day. This indicates that, under the assumed merge-point spacing and enroute recovery model, the marginal increase in waiting time becomes smaller once the departure-time error dispersion becomes sufficiently large.

The relationship between σ and coverage also provides an operational interpretation. In European A-CDM performance monitoring, the proportion of departures within ±5 min is used as a predictability-related indicator, coverage level of 85% corresponds to the fourth point from the left in this figure [3]. This point lies within the range where the RJTT curve is still increasing steeply, suggesting that the ±5 min / 85% criterion is also meaningful for Japanese airport operations. In particular, the region up to approximately σ=7.5 min, which corresponds roughly to 70% of departures falling within the ±5 min window, appears to be a high-sensitivity region for RJTT and RJFF. This suggests that maintaining departure-time prediction accuracy at least within this range may be important for limiting arrival-side airborne waiting.

Overall, the figure indicates that total airborne waiting time is highly sensitive to departure-time prediction accuracy at major arrival airports, especially RJTT and RJFF. However, because total waiting time is strongly affected by the number of arrival flights, the following subsection evaluates normalized waiting time to examine per-flight sensitivity.

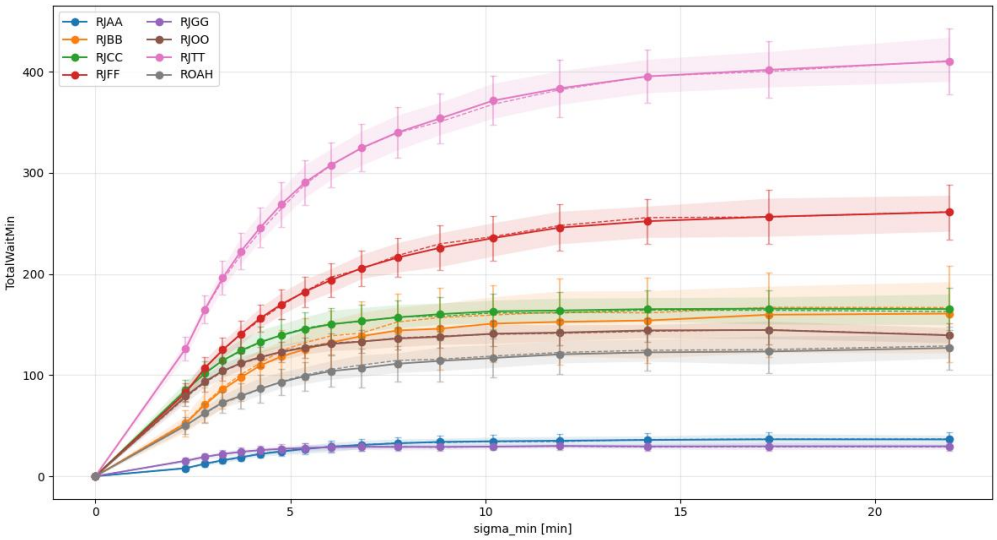


Figure 5. Airport comparison of total daily waiting time under EMG error model with 0 bias.

Figure 5 shows the corresponding results under the EMG departure-time error model with zero bias. The interpretation of the axes and plotted statistics is the same as in Figure 4. The horizontal axis represents the Gaussian standard deviation parameter σ used in the EMG calibration, and the vertical axis represents the total daily airborne waiting time in minutes.

The airport ranking is broadly consistent with the case where normal distribution was assumed (Normal case). RJTT shows the largest total waiting time, followed by RJFF and RJCC, indicating that the relative magnitude of airport-level impacts is not strongly affected by the assumed error distribution. However, the EMG curves show a steeper initial increase than the curves of Normal case. This is because the EMG distribution has a longer right tail, allowing occasional large positive departure delays even when σ is relatively small. These delays can propagate to arrival-side sequencing and generate substantial airborne waiting.

Since both the Normal and EMG models lead to similar conclusions regarding airport-level priority, the following analysis focuses on the Normal departure-time error model. The EMG results are treated as a robustness check for the effect of right-skewed departure-time errors.

5.2 Total Waiting Time and Per-Aircraft Sensitivity

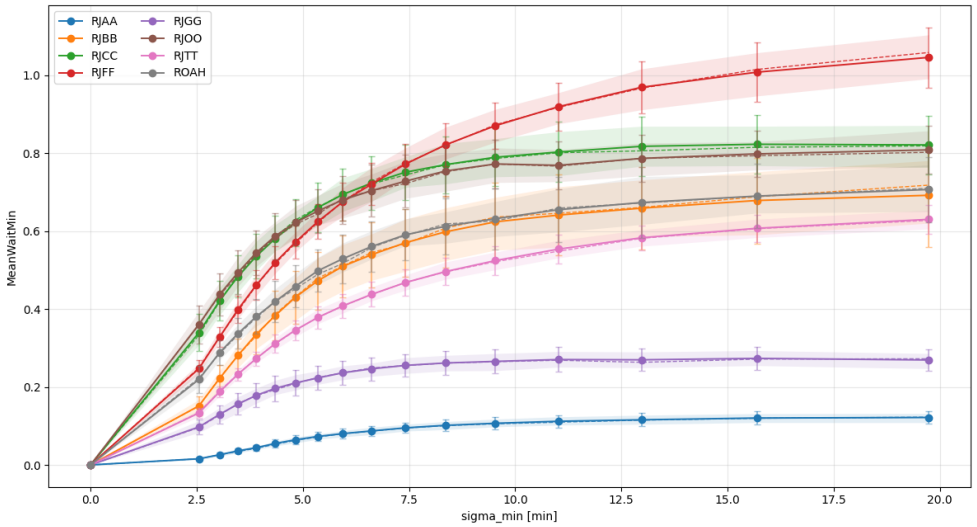


Figure 6. Airport comparison of mean airborne waiting time under Normal error model with 0 bias.

Figure 6 compares the mean waiting time normalized by traffic volume in normal case. Unlike the total waiting-time results, the normalized results indicate that RJFF and RJOO are particularly

sensitive to departure-time prediction errors. This means that even if their total waiting time is smaller than that of the highest-volume airport, each flight may experience a larger waiting-time impact when departure-time prediction accuracy deteriorates.

This contrast between total waiting time and normalized waiting time is important. RJTT has the largest aggregate impact because of its high traffic volume and dense arrival demand. In contrast, RJFF and RJOO show larger per-aircraft sensitivity, which may be related to shorter domestic routes, limited opportunity for enroute absorption, and concentrated arrival flows. The draft presentation also notes this distinction: total delay is large at RJTT and RJFF, while delay per aircraft is particularly large at RJFF and RJOO.

These results suggest that requirements for airport-specific prediction accuracy should not be evaluated only by total delay. A high-volume airport may be important from the perspective of total system benefit, while an airport with high per-aircraft sensitivity may require stricter prediction accuracy to avoid frequent airborne waiting events.

5.3 Effect of Coverage and Bias

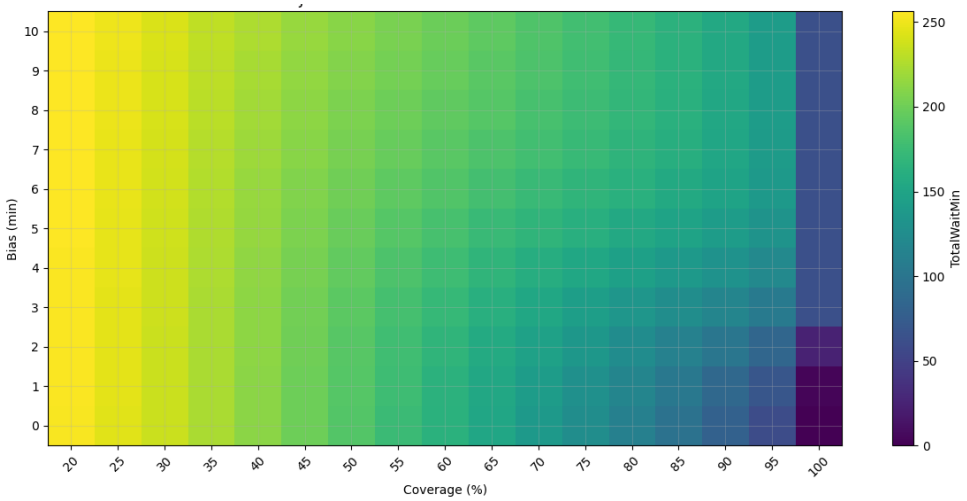


Figure 7. Relationship among coverage, bias, and total airborne waiting time for RJFF under the Normal error model.

Figure 7 shows the relationship among coverage, bias, and total airborne waiting time for RJFF under the Normal error model. The horizontal axis represents coverage, defined as the probability that the random component of the departure-time error falls within the [−5,+5] min window, while the vertical axis represents bias in minutes. The color indicates total daily airborne waiting time.

The results indicate that coverage is the dominant factor affecting waiting time. As coverage increases, the variance of departure-time errors decreases, and airborne waiting time generally decreases. Conversely, lower coverage corresponds to a larger standard deviation of the departure-time error distribution, which leads to larger residual timing errors at the arrival-side merge area and increases airborne waiting.

Bias also affects waiting time, but its influence depends on the coverage level. When coverage is high, that is, when the standard deviation of the Normal error distribution is small, the effect of bias becomes more visible. Under these conditions, the random component is relatively small, so a systematic shift in departure time can directly affect the arrival sequence. In contrast, as coverage decreases and the random dispersion becomes larger, the effect of bias becomes less distinguishable. In this low-coverage region, the magnitude of random departure-time uncertainty dominates the waiting-time outcome, and differences along with the bias direction become relatively small.

5.4 Airport-Specific Response Patterns

This section evaluates how departure-time prediction accuracy affects arrival-side airborne waiting

at each arrival airport, focusing on total waiting time and mean waiting time per aircraft. The simulation results are first compared across the eight target arrival airports. The objective is to distinguish airports with large aggregate waiting-time impacts from those with high per-aircraft sensitivity.

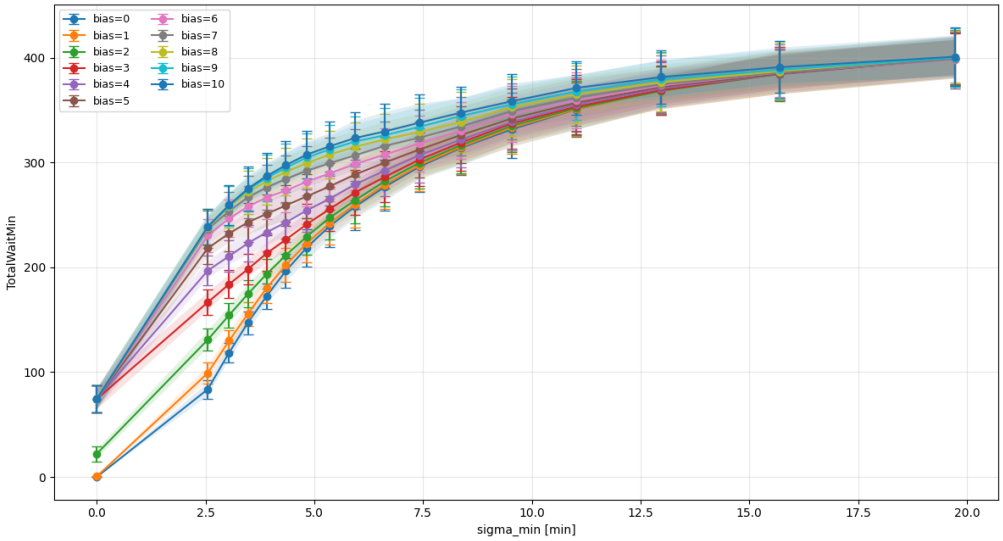


Figure 8. Total daily airborne waiting time for RJTT by bias level under the Normal error model.

Figure 8 shows the total daily airborne waiting time for RJTT under the Normal error model. The horizontal axis represents the standard deviation σ of the departure-time error distribution, and each line corresponds to a different bias level. The total waiting time increases rapidly as σ increases from zero and then gradually approaches approximately 400 min per day.

The effect of bias is most visible when σ is small, corresponding to high coverage. In this region, the random component of the departure-time error is limited, so systematic bias has a relatively large influence on arrival-side sequencing. However, as σ increases, the curves for different bias levels become closer to each other. This indicates that, under low-coverage conditions, random dispersion dominates the total waiting-time outcome and the additional effect of bias becomes relatively small.

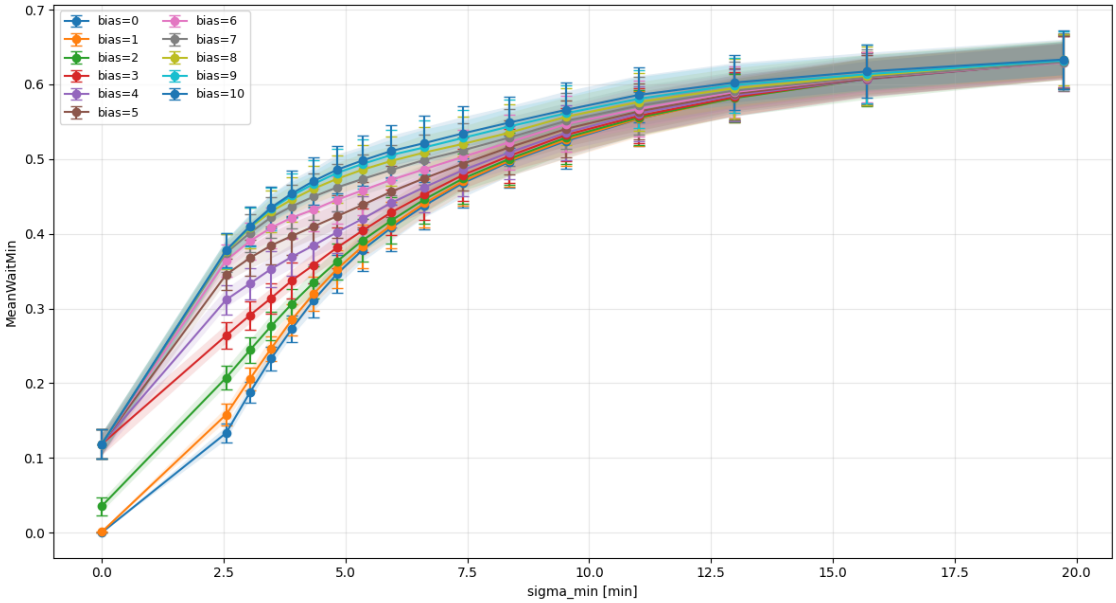


Figure 9. Mean airborne waiting time for RJTT by bias level under the Normal error model.

Figure 9 shows the mean airborne waiting time for RJTT under the same conditions as Figure 9.

The horizontal axis again represents the standard deviation σ of the departure-time error distribution, while the vertical axis represents mean waiting time. The mean waiting time increases with σ and gradually approaches approximately 0.64 min.

The overall trend is similar to that of the total waiting-time result, but Figure 10 normalizes the impact by the number of waiting events or flights represented in the simulation output. Therefore, it provides a complementary view of how strongly each arrival is affected by departure-time uncertainty. As in Figure 9, the bias effect is clearer in the small-σ region and becomes less distinguishable as σ increases.

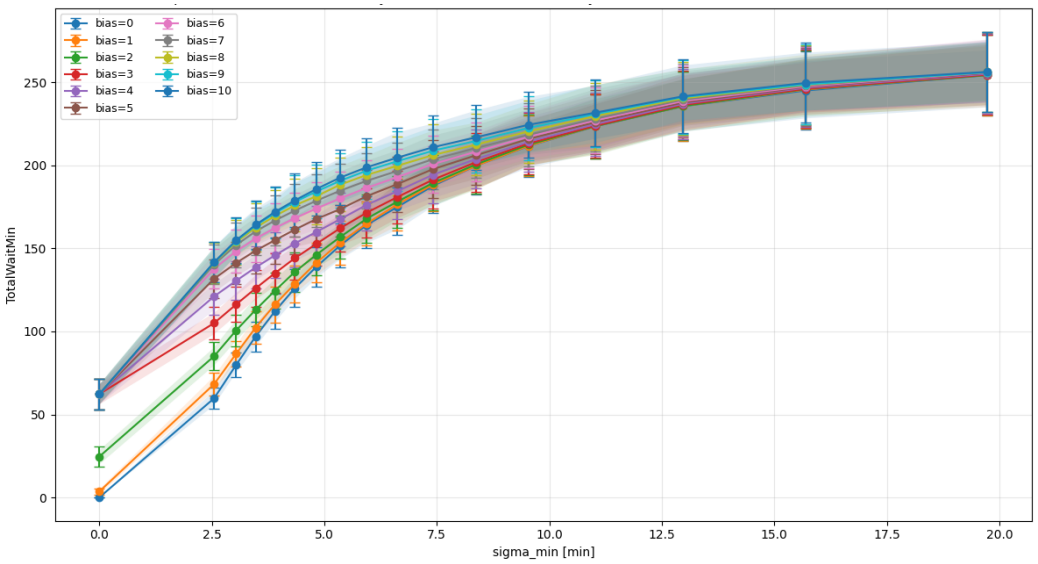


Figure 10. Total daily airborne waiting time for RJFF by bias level under the Normal error model.

Figure 10 shows the total daily airborne waiting time for RJFF under the Normal error model. As in Figure 9, the horizontal axis represents the standard deviation σ of the departure-time error distribution, and each line corresponds to a different bias level.

The overall trend is similar to that observed for RJTT. Total waiting time increases rapidly as σ increases from zero, and the effect of bias is most visible in the small-σ region, where coverage is high. As σ becomes larger, the curves for different bias levels converge, indicating that random dispersion becomes the dominant factor and the relative influence of bias decreases.

The main difference from RJTT is the magnitude of the total waiting time. While RJTT approaches approximately 400 min per day, RJFF approaches approximately 250 min per day. This indicates that RJFF has a smaller aggregate waiting-time impact than RJTT, but still shows substantial sensitivity to departure-time prediction errors. Therefore, RJFF should also be considered an important arrival airport when discussing airport-specific prediction accuracy requirements.

Figure 11 shows the mean airborne waiting time for RJFF under the Normal error model. The horizontal axis represents the standard deviation σ of the departure-time error distribution, and each line corresponds to a different bias level. The overall response pattern is similar to the total waiting-time result: mean waiting time increases as σ increases, and the influence of bias becomes less distinguishable in the large-σ region.

A notable difference from RJTT is the magnitude of the normalized waiting-time impact. The mean waiting time at RJFF approaches approximately 1.0 min, which is larger than the corresponding value for RJTT. This suggests that, although RJFF has a smaller total waiting-time impact than RJTT, each arrival flight is more strongly affected by departure-time uncertainty.

This higher normalized sensitivity may be related to two factors. First, compared with RJTT, a larger proportion of flights arriving at RJFF may consist of domestic flights, which generally have shorter flight distances and therefore less opportunity for enroute recovery of departure-time errors. Second, RJFF has fewer landing runways than RJTT. In the queueing representation used in this study, this corresponds to a smaller number of service lanes for processing arrival traffic, making

waiting more likely to occur when arrival times are perturbed. These factors may explain why RJFF shows a higher mean waiting-time impact even though its total waiting time is smaller than that of RJTT.

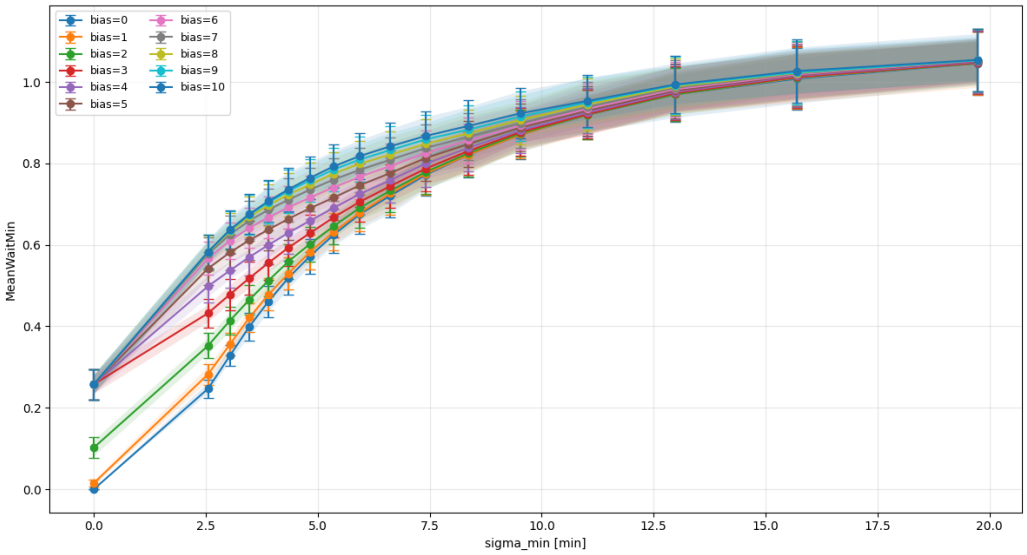


Figure 11. Mean airborne waiting time for RJFF by bias level under the Normal error model.

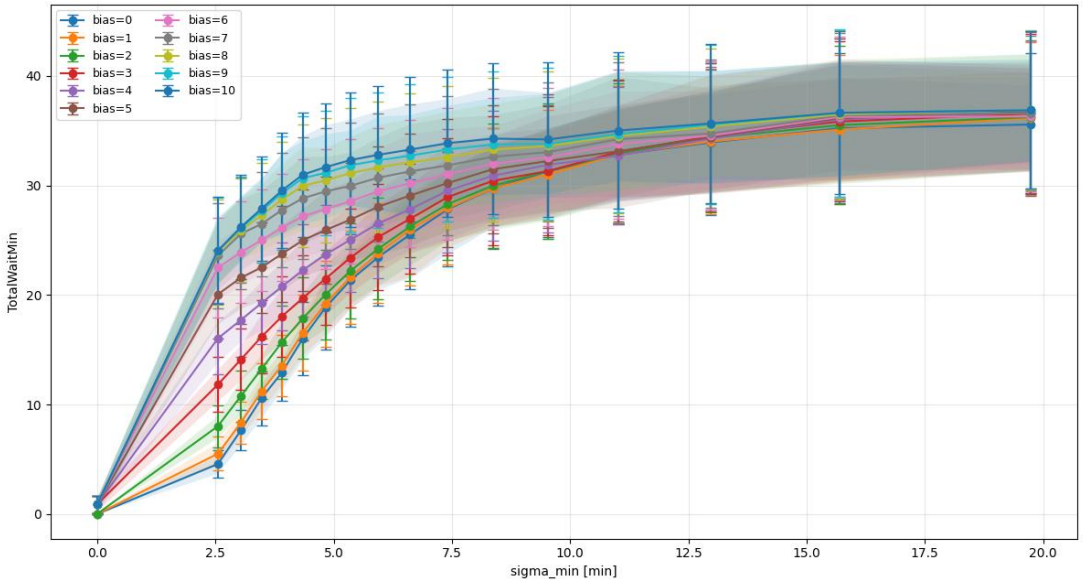


Figure 12. Total daily airborne waiting time for RJAA by bias level under the Normal error model.

Figure 12 shows the total daily airborne waiting time for RJAA under the Normal error model. Compared with RJTT and RJFF, the total waiting time at RJAA is much smaller, remaining around 40 min per day even in the large-σ region. This indicates that departure-time prediction errors have a relatively limited aggregate impact on RJAA under the assumptions of this study.

The relative variability is larger than that of RJTT or RJFF, as the error bars and interquartile bands occupy a larger portion of the mean value. This suggests that RJAA results are more sensitive to day-to-day traffic composition and the random realization of departure-time errors.

A possible explanation is that RJAA has a large share of international arrival traffic. Because the simulation applies distance-based enroute recovery, longer flights can absorb a larger portion of departure-time errors before reaching the arrival-side merge area.

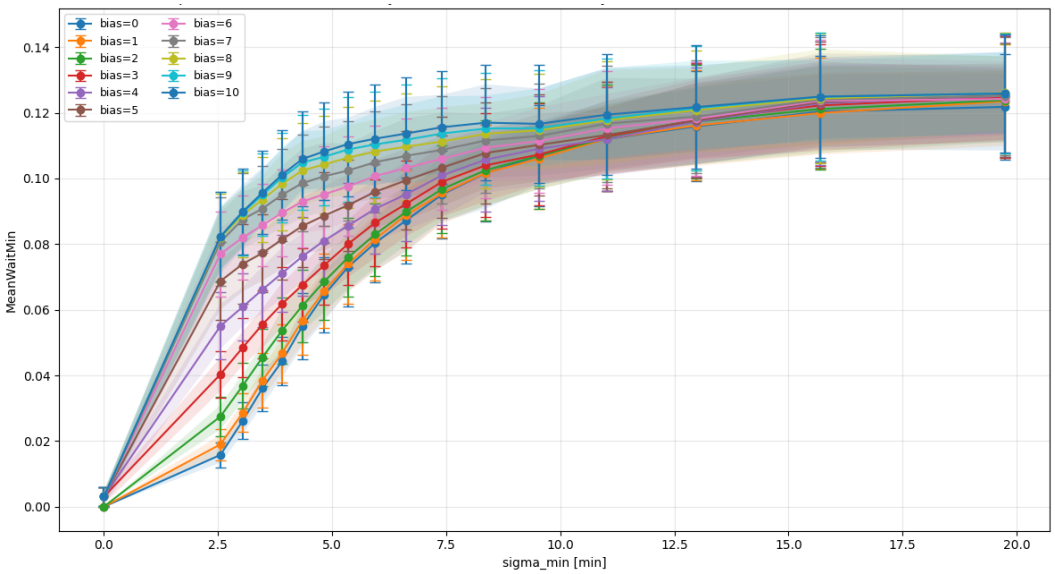


Figure 13. Mean airborne waiting time for RJAA by bias level under the Normal error model.

Figure 13 shows the mean airborne waiting time for RJAA under the Normal error model. The mean waiting time is relatively small compared with RJTT and RJFF, gradually approaching approximately 0.12 min. This indicates that the normalized impact of departure-time uncertainty on RJAA arrival traffic is limited under the present assumptions.

In the small-σ region, especially below approximately 5 min, the difference among bias levels is relatively clear. This suggests that when random dispersion is small, systematic bias can have a larger influence on RJAA waiting time than coverage. In other words, for RJAA arrival traffic, the overall timing shift of the departure-time error distribution may become more important once departure-time uncertainty is already sufficiently limited.

This may be partly because longer-distance flights can recover small-to-moderate timing errors under the distance-based enroute recovery model. As a result, the residual random error at the arrival-side merge point is reduced, making the effect of systematic bias more visible.

Overall, these airport-specific response patterns indicate that the relationship between departure-time prediction accuracy and arrival-side waiting is not uniform across airports. RJTT is important from the perspective of total system impact, while RJFF and RJOO are important from the perspective of normalized or per-flight sensitivity. These differences support the need for airport-specific accuracy requirements rather than a single uniform prediction-accuracy target.

6. Impact of Departure-Airport Predictability on Downstream Arrival Waiting

6.1 Purpose and Method of Departure-Airport Attribution

The results in Section 5 evaluated the sensitivity of airborne waiting from the perspective of arrival airports. However, departure-time prediction accuracy is primarily improved at the departure airport, through better milestone management, surface operation monitoring, information sharing, and prediction systems. Therefore, arrival-airport results alone do not directly indicate where prediction accuracy improvements should be prioritized.

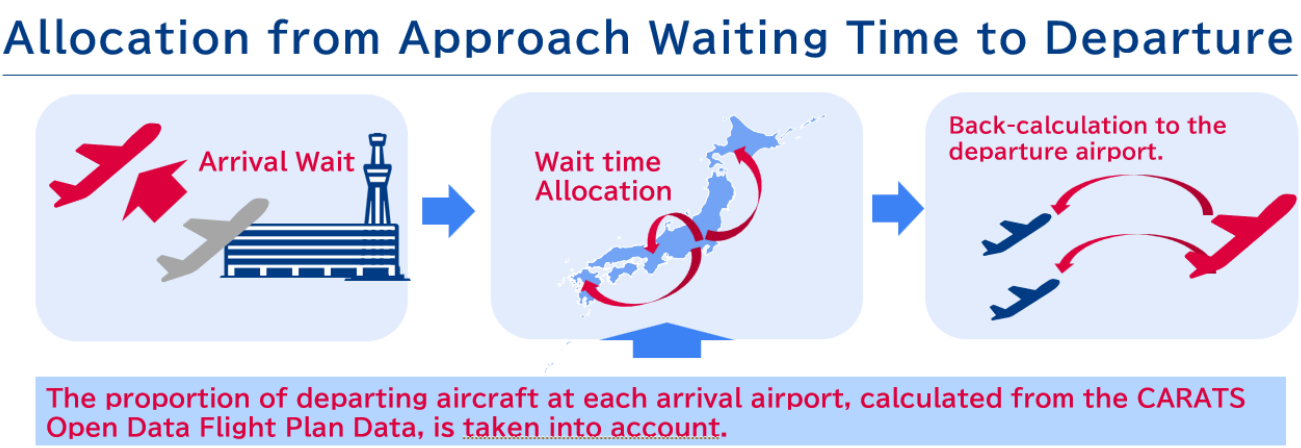


Figure 14. Concept of departure-airport attribution.

To address this issue, this study attributes arrival-side airborne waiting back to departure airports, as illustrated in Figure 14. The attribution is conducted as a post-processing step using an airport-pair traffic-share matrix. Let $W_{r,s}$ denote the airborne waiting time generated at arrival airport r under scenario s, and let $q_{r,d}$ denote the share of flights arriving at airport r that departed from departure airport d. The waiting time allocated to departure airport d is then calculated as

$$W_{d,s}^{alloc} = \sum_{r} q_{r,d} W_{r,s} \tag{9}$$

This formulation does not assume that the arrival-side waiting physically occurs at the departure airport. Rather, it estimates how much of the arrival-side waiting impact is associated with traffic originating from each departure airport. In this sense, the attribution provides an operational interpretation of where departure-time predictability improvements may be most effective.

The same allocation procedure is applied to both total waiting time and mean waiting time. Total allocated waiting time represents the aggregate contribution of each departure airport to arrival-side waiting, while mean allocated waiting time provides a normalized indicator of the relative impact associated with each departure airport. For the annual visualization, seed-level results are first averaged by day for each scenario, and daily outliers are removed using the IQR rule before calculating annual statistics.

In this section, the attribution results are shown for the Normal error model with zero bias. The horizontal axis represents the standard deviation σ of the departure-time error distribution. A larger σ corresponds to lower departure-time prediction accuracy, or equivalently lower coverage within the [−5,+5] min tolerance window.

This post-processing step allows the analysis to move from the question of “which arrival airports are sensitive to departure-time errors?” to the more operational question of “which departure airports are associated with larger downstream arrival-side waiting impacts under departure-time uncertainty.

6.2 Total Attributed Waiting Time by Departure Airport

Figure 15 shows the total allocated waiting time by departure airport. The results indicate that Tokyo International Airport (RJTT) has by far the largest attributed waiting time across the tested range of prediction uncertainty. As the standard deviation increases, the waiting time attributed to RJTT rises rapidly and then gradually approaches a plateau. This indicates that departure-time uncertainty at RJTT-related flows has a large aggregate impact on arrival-side waiting.

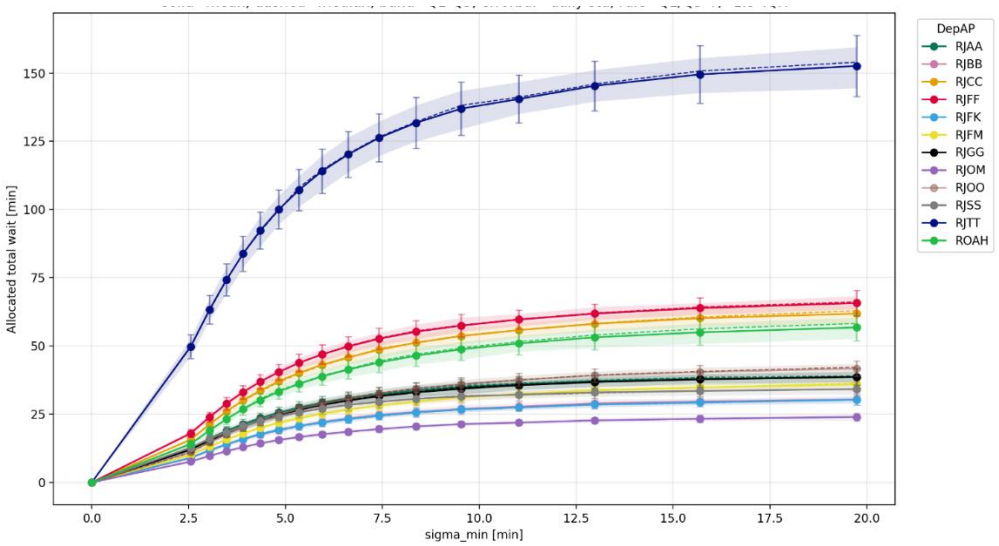


Figure 15. Total allocated waiting time by departure airport under Normal error model with 0 bias.

Other departure airports show smaller but non-negligible impacts. Fukuoka Airport (RJFF), New Chitose Airport (RJCC), and Naha Airport (ROAH) also show relatively large total attributed waiting time compared with the other airports. This suggests that the system-level benefit of improving departure-time predictability is not limited to the largest airport, although RJTT is clearly dominant in total impact.

The strong contribution of RJTT is likely explained by its large traffic volume and its role as a major airport in domestic traffic flows. Since total attributed waiting time is affected by both the number of departing flights and the sensitivity of their destination flows, high-volume departure airports naturally tend to have larger aggregate impacts.

6.3 Mean Attributed Waiting Time

Figure 16 shows the mean allocated waiting time by departure airport. The horizontal axis represents the standard deviation σ of the Normal departure-time error distribution, and the vertical axis represents the mean allocated waiting time per flight-equivalent. The solid lines indicate the mean values after IQR-based outlier filtering, the dashed lines indicate the median values, the shaded bands show the interquartile range, and the error bars show the daily standard deviation.

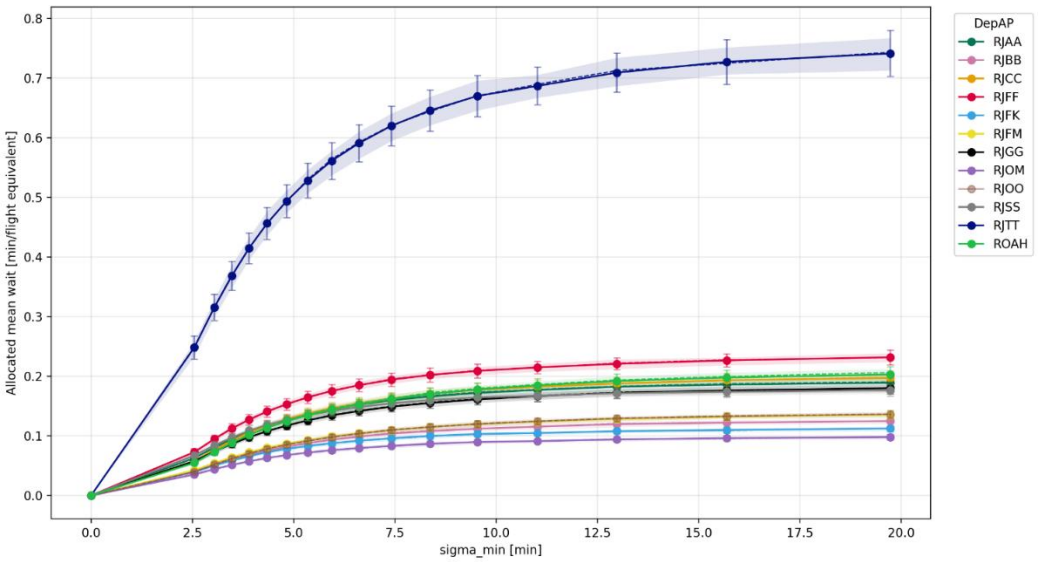


Figure 16. Mean allocated waiting time by departure airport under Normal error model with 0 bias.

The results show that RJTT has by far the largest mean allocated waiting time across the tested

range of prediction uncertainty. The value approaches approximately 0.7 min per flight-equivalent in the large-σ region. This indicates that departure-time predictability at RJTT is the most important among the evaluated departure airports, not only from the perspective of total traffic volume but also from the perspective of normalized downstream impact.

One possible reason is that RJTT is a major origin airport for flights bound for arrival airports that showed high per-flight sensitivity in Section 5, such as RJFF and RJCC. Therefore, departure-time errors at RJTT-related flows can propagate to arrival-side merge-point sequencing at sensitive destination airports. This may explain why RJTT remains dominant even after normalizing the allocated waiting impact.

The sensitivity of RJTT is especially high in the small- to medium-σ range. Up to approximately σ=5.0 min, which corresponds roughly to a state where about 70% of aircraft fall within the ±5 min tolerance window, the mean allocated waiting time increases almost linearly. This suggests that, for RJTT, improving departure-time prediction coverage within this range can have a substantial marginal effect on reducing downstream airborne waiting.

RJFF shows the second-largest mean allocated waiting time, although its impact is much smaller than that of RJTT. This result is consistent with the arrival-airport analysis in Section 5, where Fukuoka-related flows showed high sensitivity to departure-time prediction errors. Airports such as RJCC, ROAH, RJAA, RJGG, RJSS, and RJOO show moderate impacts, while RJOM and RJBB remain relatively low under the tested scenarios.

These results provide a direct basis for prioritizing investments in departure-time prediction improvement. The sensitivity curves quantify the benefit side of the decision problem: for each departure airport, they indicate how much downstream airborne waiting can be reduced by improving prediction coverage. For example, if an operational measure improves coverage by one step, the expected reduction in allocated waiting time can be read from the slope of the corresponding curve in Figure 16.

From this perspective, RJTT should have first priority for improving departure-time predictability, followed by RJFF. The marginal benefit of improving prediction accuracy at RJTT is substantially larger than that at other departure airports, especially in the small- to medium-σ range. Therefore, if the cost of improving coverage by a given amount is comparable across airports, investment at RJTT would produce the largest reduction in downstream airborne waiting.

In practical decision-making, the remaining information required is the implementation cost. Once vendors or system operators provide the cost of improving departure-time prediction coverage, for example by 5 percentage points, the benefit estimated from Figure 16 can be directly compared with that cost. This enables A-CDM-related investments to be evaluated not only qualitatively but also quantitatively, using airport-specific marginal benefits. In this sense, the proposed framework converts departure-time prediction accuracy from a general operational objective into a measurable investment target.

7. Limitation

Several limitations should be noted. First, the arrival-side constraint is represented by simplified merge-point spacing rather than by detailed runway configuration, wake turbulence separation, airport acceptance rate, or controller workload. This simplification was adopted because official capacity and workload parameters are not publicly available. Therefore, the absolute waiting-time values should be interpreted with caution. The main contribution of the simulation is the relative sensitivity comparison across airports and prediction-accuracy conditions.

Second, enroute absorption is modeled using a simplified distance-based rule. In actual operations, the ability to absorb timing errors depends not only on flight distance but also on aircraft type, wind, cruise altitude, airspace constraints, route availability, schedule buffer, and controller intervention. The current model captures the general assumption that longer flights have more opportunity to absorb timing errors, but further refinement would be necessary for operational implementation.

Third, the no-waiting benchmark is an idealized reference schedule. It is useful for isolating the effect of departure-time prediction errors, but it does not represent actual ATFM operations in full

detail. In practice, ground delay, tactical sequencing, speed control, and arrival management would interact dynamically. Future work should compare the benchmark-based sensitivity results with more operationally detailed simulations or observed delay data.

Finally, the current analysis focuses on airborne waiting time as the primary indicator. Sector-count indicators were implemented as optional supplementary outputs, but they were not used as the main performance measure in this paper. Future research should extend the framework to include more detailed airspace congestion indicators, sector workload proxies, fuel burn, CO_2 emissions, and passenger delay impacts. These extensions would allow a more comprehensive cost-benefit evaluation of A-CDM and trajectory-based operation improvements.

Despite these limitations, the proposed framework provides a practical way to estimate airport-specific departure-time prediction accuracy requirements. It can support evidence-based prioritization by identifying where improved predictability is likely to produce the largest operational benefit. In this sense, the framework can contribute to future A-CDM deployment, data-sharing strategies, and trajectory-based operation planning in Japan.

8. Conclusion

This study developed a fast-time simulation framework to evaluate how departure-time prediction accuracy affects arrival-side airborne waiting time at Japanese airports. Using flight plan data stored in CARATS Open Data, the framework reconstructs waypoint-level trajectories, constructs an iterative no-waiting benchmark, introduces stochastic departure-time errors, applies distance-based enroute recovery, and calculates waiting time through event-based merge-point queueing simulation. Prediction accuracy was represented by coverage, defined as the probability that the random component of the departure-time error falls within a specified tolerance window.

The arrival-airport analysis showed that the impact of departure-time prediction errors differs substantially across airports. Under the Normal error model with zero bias, RJTT had the largest aggregate impact, with total waiting time approaching approximately 400 min/day, followed by RJFF at approximately 250 min/day. In contrast, normalized waiting-time results showed that RJFF and RJOO are particularly sensitive on a per-flight basis. RJFF showed a mean waiting time approaching approximately 1.0 min, which was larger than the corresponding value for RJTT, while RJAA showed a relatively small impact. These results demonstrate that total waiting time and mean waiting time provide different but complementary perspectives for airport-specific accuracy requirements.

The sensitivity analysis also showed that coverage is a key driver of airborne waiting time. In general, lower coverage, or larger departure-time error variance, increased both total and mean waiting time. Bias was more influential in the high-coverage region, where random dispersion was small, but its relative effect decreased as coverage became lower and random uncertainty became dominant. The EMG results confirmed that right-skewed departure-time errors can generate a steeper initial increase in waiting time, while the relative ranking of airports remained broadly consistent with the Normal case. Therefore, the main conclusions regarding airport priority are robust to the assumed distributional shape.

The departure-airport attribution analysis provided an additional operational interpretation. By allocating arrival-side waiting back to departure airports using an airport-pair traffic-share matrix, the analysis identified where prediction-accuracy improvements may be most effective. RJTT was the dominant departure airport in both total and mean allocated waiting time, and RJFF showed the next largest normalized impact. In particular, the mean allocated waiting time for RJTT increased almost linearly up to approximately σ=5.0 min, corresponding roughly to 70% coverage within the ±5 min window. This indicates that improving departure-time prediction coverage at RJTT can have a substantial marginal effect on reducing downstream airborne waiting.

The main contribution of this study is to convert departure-time prediction accuracy from a general operational objective into a measurable investment target. The sensitivity curves quantify the benefit side of prediction-accuracy improvement: for each departure airport, they show how much downstream airborne waiting can be reduced by improving coverage. Once the implementation cost of improving coverage is obtained from system vendors or airport operators, the benefit estimated

by the proposed framework can be directly compared with that cost. This enables evidence-based prioritization of A-CDM-related investments, with RJTT as the first priority and RJFF as the next important candidate under the present assumptions.

Several limitations remain. The arrival-side constraint is represented by simplified merge-point spacing, enroute recovery is modeled using a distance-based rule, and the no-waiting benchmark is an idealized reference schedule. Therefore, the absolute waiting-time values should be interpreted with caution, while the relative sensitivity comparison across airports and prediction-accuracy conditions is the main contribution. Future work will refine the arrival-side capacity model, improve the enroute recovery model, extend the evaluation period, and incorporate additional indicators such as sector congestion, fuel consumption, emissions, and passenger delay. These extensions will support a more comprehensive assessment of the operational benefits of improved departure-time prediction accuracy under A-CDM and trajectory-based operations.

Contact Author Email Address

Corresponding author: Yota Iwatsuki
Email: yota_iwatsuki@mri.co.jp
Alternative email: iwatsukiyota@gmail.com

Copyright Statement

The authors confirm that they, and/or their company or organization, hold copyright on all of the original material included in this paper. The authors also confirm that they have obtained permission, from the copyright holder of any third party material included in this paper, to publish it as part of their paper. The authors confirm that they give permission, or have obtained permission from the copyright holder of this paper, for the publication and distribution of this paper as part of the ICAS proceedings or as individual off-prints from the proceedings.

References

[1] International Air Transport Association, Global Outlook for Air Transport: Highly Resilient, Less Robust, 2023.URL: https://www.iata.org/en/iata-repository/publications/economic-reports/global-outlook-for-air-transport----june-2023/

[2] EUROCONTROL, Airport Collaborative Decision-Making (A-CDM) Implementation Manual, 2017.URL: https://www.eurocontrol.int/publication/airport-collaborative-decision-making-cdm-implementation-manual

[3] EUROCONTROL, A-CDM Impact Assessment Final Report, 2016.URL: https://www.eurocontrol.int/sites/default/files/2019-04/a-cdm-impact-assessment-2016.pdf

[4] ICAO Sixth Meeting of the Asia/Pacific Airport Collaborative Decision Making Task Force (APA-CDM/TF/6), PROGRESS OF A-CDM IMPLEMENTATION IN JAPAN. https://www.icao.int/sites/default/files/APAC/Meetings/2021/2021%20APA-CDM%20TF6/4-Information%20Papers/IP03-AI-3_REV-1-Progress-of-A-CDM-implemention-in-Japan_Clean.pdf

[5] R. Dalmau, A. Trzmiel, and S. Kirby, “PETA: Combining Machine Learning Models to Improve Estimated Time of Arrival Predictions,” SESAR Innovation Days, 2023.URL: https://www.sesarju.eu/sites/default/files/documents/sid/2023/Papers/SIDs_2023_paper_53%20final.pdf

[6] A. Andreeva-Mori, “Quantifying Effects of Departure Time Uncertainty on Ground Delay Program Control Parameters,” Transactions of the Japan Society for Aeronautical and Space Sciences, Vol. 68, No. 5, 2025.URL: https://www.jstage.jst.go.jp/article/tjsass/68/5/68_T-24-46/_article

[7] A. Andreeva-Mori, Y. Matsuno, and N. Matayoshi, “Departure Control Time Considering the Cost of Airborne Delay and Ground Delay,” Journal of the Japan Society for Aeronautical and Space Sciences, Vol. 68, No. 1, pp. 31–37, 2020.URL: https://www.jstage.jst.go.jp/article/jjsass/68/1/68_68_31/_article/-char/ja

[8] A. Andreeva-Mori and Y. Matsuno, “Impact ofenroute Time-Based Metering on Equity in Delay Distribution,” Proceedings of the 32nd Congress of the International Council of the Aeronautical Sciences, 2021.URL: https://www.icas.org/icas_archive/ICAS2020/data/papers/ICAS2020_0202_paper.pdf

[9] Y. Matsuno and A. Andreeva-Mori, “Feasibility Analysis of Time-Based Metering Using Cruise-Speed Control and Flight-Level Change for Domestic Flights in Japan,” Transactions of the Japan Society for

Aeronautical and Space Sciences, Vol. 65, No. 4, pp. 139–146, 2022.URL: https://www.jstage.jst.go.jp/article/tjsass/65/4/65_T-21-20/_article/-char/ja/

[10]A. Motodani and N. Takeichi, “Modeling of Flight Time Uncertainty in 4D Trajectory Management,” Journal of the Japan Society for Aeronautical and Space Sciences, Vol. 65, No. 3, pp. 130–134, 2017.URL: https://www.jstage.jst.go.jp/article/jjsass/65/3/65_65_130/_pdf

[11]Civil Aviation Bureau, Ministry of Land, Infrastructure, Transport and Tourism, Japan, CARATS Open Data.URL: https://www.mlit.go.jp/koku/carats/get-open-data/

[12]J. W. Tukey, Exploratory Data Analysis, Addison-Wesley, 1977.Available at: https://archive.org/details/exploratorydataa0000tuke_7616